Chinese Chemical Letters 29 (2018) 582–586

Contents lists available at ScienceDirect

Chinese Chemical Letters

journal homepage: www.elsevier.com/locate/cclet

Communication

Simplified fabrication of high areal capacitance all-solid-state micro-supercapacitors based on graphene and MnO_2 nanosheets

Jieqiong Qin[a,c], Zhong-Shuai Wu[a,*], Feng Zhou[a], Yanfeng Dong[a], Han Xiao[a], Shuanghao Zheng[a,b,c], Sen Wang[a,c], Xiaoyu Shi[a,b,d], Haibo Huang[a], Chenglin Sun[a], Xinhe Bao[a,b]

[a] Dalian National Laboratory for Clean Energy, Dalian Institute of Chemical Physics, Chinese Academy of Sciences, Dalian 116023, China
[b] State Key Laboratory of Catalysis, Dalian Institute of Chemical Physics, Chinese Academy of Sciences, Dalian 116023, China
[c] University of Chinese Academy of Sciences, Beijing 100049, China
[d] Department of Chemical Physics, University of Science and Technology of China, Hefei 230026, China

ARTICLE INFO

Article history:
Received 18 May 2017
Received in revised form 2 August 2017
Accepted 4 August 2017
Available online 12 August 2017

Keywords:
MnO_2 nanosheets
Graphene
All-solid-state
Planar
Micro-supercapacitors
Energy storage

ABSTRACT

All-solid-state micro-supercapacitors are acknowledged as a very promising class of microscale energy storage devices for directly integrating portable and wearable electronics. However, the improvement of electrochemical performance from materials to devices still remains tremendous challenges. Here, we demonstrate a novel and universal mask-assisted filtration technology for the simplified fabrication of all-solid-state planar micro-supercapacitors (MSCs) based on interdigital patterns of 2D pseudocapacitive MnO_2 nanosheets and electrochemically exfoliated graphene film as both electrode and current collector, and polyvinyl alcohol/LiCl gel as electrolyte. Remarkably, the resulting MSCs exhibit outstanding areal capacitance of ~355 mF/cm^2, which is among the highest values reported in the state-of-the-art MSCs. Meanwhile, MSCs possess exceptionally mechanical flexibility as high as ~92% of initial capacitance even at a highly bending angle of 180°, excellent cyclability with a capacitance retention of 95% after 3000 cycles, and impressive serial or parallel integration for modulating the voltage or capacitance. Therefore, our proposed strategy of simplified construction of MSCs will pave the ways for utilizing graphene and analogous pseudocapacitive nanosheets in high-performance MSCs.

With the rapid development of wearable and portable electronics, microscale energy storage devices with multiple compatible features of lightweight, tailored size, outstanding flexibility, and high energy density have gained tremendous attentions. Recently, micro-supercapacitors (MSCs) are considered as a very promising class of on-chip energy storage devices for integrated electronics due to ultrahigh power delivery, excellent rate capability, robust mechanical flexibility, unique shape diversity and safety [1–3]. Despite remarkable advancements in the fabrication of nanostructured electrode materials and the manufacturing of novel devices, there are still huge challenges in the development of MSCs with high areal capacitance, which is a crucial performance metrics of MSCs [4,5]. To boost the areal capacitance, the key is to develop high-performance thick electrode materials with developed ionic and electronic conducting network, which however is still underdeveloped in this important research field.

Two-dimensional (2D) materials, characterized by nanoscale dimension in thickness and infinite length in the plane, are currently regarded as groundbreaking electrode candidates for MSCs because they present unique properties of large surface area, ultra-thinness, high mechanical flexibility, and unprecedented capacitance characteristics, and also demonstrate potential applications in electronics, transparent conducting electrode, composites, energy storage and conversion [6–10]. Conceptually, 2D materials mainly include graphene and graphene-like analogues (such as, transition metal oxides/hydroxides, metal sulfides, boron nitride, MXenes, phosphorene, thiophene) [11–13]. Among them, MnO_2 nanosheets have received extensive concerns for high-performance supercapacitors because of high surface area, inexpensive massive scalability, high theoretical capacity (1370 F/g), environmentally friendly merit, and natural abundance [14,15]. However, MnO_2 intrinsically suffers from low electrical conductivity, resulting in poor rate capability and power density

* Corresponding author.
E-mail address: wuzs@dicp.ac.cn (Z.-S. Wu).

http://dx.doi.org/10.1016/j.cclet.2017.08.007

[16,17]. To overcome this issue, MnO_2 hybrids with highly conductive materials, *e.g.*, graphene, carbon nanotube, were usually proposed as electrodes for supercapacitors [18–22]. From these viewpoints, one promising method for fabricating MSCs is to manufacture compact film electrodes constructed by 2D pseudocapacitive MnO_2 nanosheets and capacitive conducting graphene, which may dramatically enhance the electrochemical performance of MSCs. Moreover, the conventional device manufacturing of planar MSCs by photolithographic techniques normally involved complicated processing (*e.g.*, spin-coating photoresist, baking, masked irradiation, development), O_2 plasma etching, and sputtering metal-based current collectors (*e.g.*, Au), which significantly hindered large-scale and low-cost production of MSCs [23,24]. Nevertheless, simplified construction of interdigital planar electrodes from ultrathin MnO_2 nanosheets and graphene for flexible MSCs has not yet been reported.

Herein, we demonstrate the simplified fabrication of all-solid-state planar MSCs (denoted as MG-MSCs) with high areal capacitance, based on interdigital patterned films (MG) of 2D pseudocapacitive MnO_2 nanosheets and electrochemically exfoliated graphene (EG), using polyvinyl alcohol/LiCl (PVA/LiCl) gel as electrolyte. The MG films with interdigital patterns were directly fabricated through a step-by-step filtration of high-conducting EG nanosheets acting as current collectors firstly, followed by depositing a hybrid film of 2D MnO_2 nanosheets and EG as electrodes with the assistance of a customized mask on Nylon membrane. The resulting MG hybrid film showed excellent uniformity, flexibility, and electrical conductivity (84 S/cm), which can be directly served as binder- and additive-free flexible electrodes for MSCs. Remarkably, the fabricated MG-MSCs exhibited high areal capacitance of ~355 mF/cm^2, outstanding mechanical flexibility with ~92% of initial capacitance even at a highly bending angle of 180°, and pronounced cycling stability of 95% after 3000 cycles. In addition, MG-MSCs could efficiently realize designable integrated power source pack through parallel and serial interconnection, delivering high output current and voltage. Therefore, this simplified fabrication strategy using graphene and analogous nanosheets as electrodes and current collectors may open up numerous opportunities for developing high-performance MSCs.

The fabrication process of MG-MSCs is schematically depicted in Fig. 1. Briefly, three key steps were included as follows. First, EG interdigital patterns was manufactured as current collectors by filtration of EG dispersion, with assistance of the customized mask. Second, the MG hybrid interdigital patterns as electrodes were directly prepared by deposition of 2D MnO_2 and EG dispersion on a nylon membrane. Third, MG-MSCs based on MG films with tailored thickness were achieved after drop-casting and solidification of PVA/LiCl electrolyte.

To assemble high areal capacitance MG-MSCs, 2D pseudocapacitive MnO_2 nanosheets and capacitive EG nanosheets with

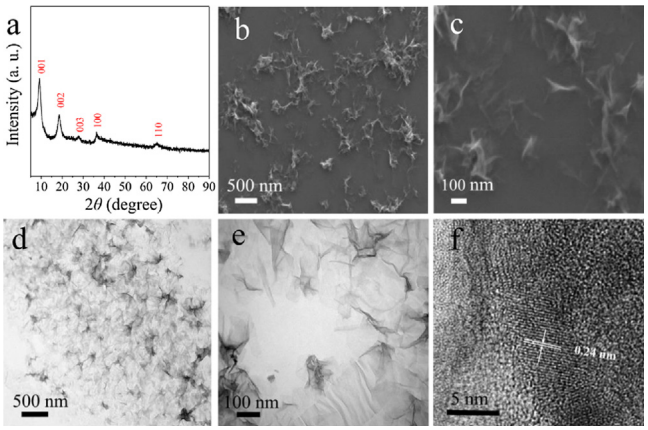

Fig. 2. (a) XRD patterns, (b, c) SEM, (d, e) TEM, and (f) HRTEM images of MnO_2 nanosheets.

outstanding electrical conductivity were chosen. Specifically, the MnO_2 nanosheets were synthesized by chemical oxidation of Mn^{2+} ions with tetramethylammonium hydroxide (TMA•OH) [25,26]. The crystal structure of the as-prepared MnO_2 nanosheets was confirmed by XRD pattern, in which all the diffraction peaks located at 9.2°, 18.5°, 27.8°, 36.3° and 65.1° were well attributed to the (001), (002), (003), (100) and (110) crystal faces of MnO_2, respectively (Fig. 2a) [25,27]. SEM and TEM images (Figs. 2b–f) presented that the MnO_2 nanosheets were ultrathin, flat, and transparent graphene-like structure. As shown in Fig. 2f, HRTEM image confirmed the well-crystalline phase with lattice distance of ~0.24 nm, which was assigned to the (100) plane. The EG nanosheets prepared by electrochemical exfoliation of graphite possessed flat and uniform morphology, large lateral size (~10 μm), ultrathin layer (≤5 layers) and high solution process ability (Fig. S1 in Supporting information), which were benefit for the formation of large-area and conductive films.

MG-MSCs were readily fabricated by mask-assisted filtration of high-conducting EG nanosheets firstly, followed by depositing a hybrid film of 2D MnO_2 nanosheets and EG as electrodes on Nylon membrane (Figs. 3a and b), using PVA/LiCl gel as electrolyte. Notably, the resulting interdigital patterned MG hybrid films showed excellent uniformity, and good mechanical flexibility (Figs. 3a and b), and can be directly served as binder- and additive-free electrodes for MG-MSCs, in which the first-deposited EG layer can act as current collectors, instead of metal-based current collectors. Further, top-view SEM images of MG films revealed good structural integrity of EG and MnO_2 nanosheets, large-area continuity and uniformity with flat surface, which demonstrated that this technique was highly favorable for the construction of flexible MG-MSCs (Fig. 3c). Cross-section SEM images of MG film clearly exhibited layer-stacked structure of graphene and MnO_2

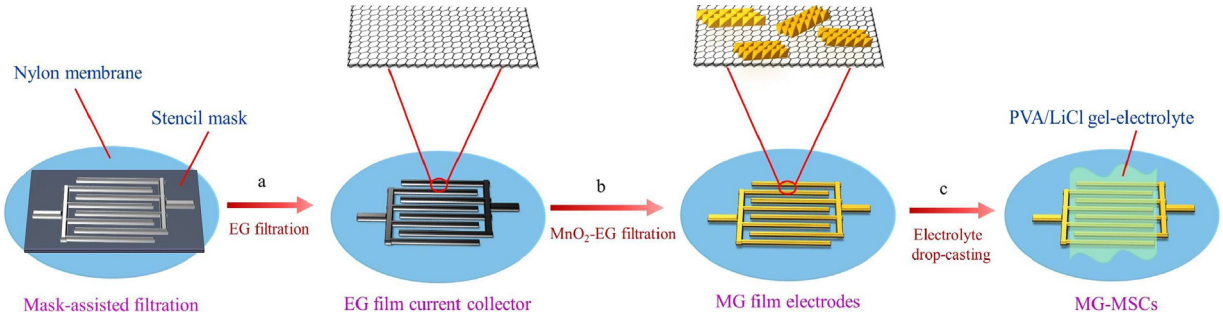

Fig. 1. Schematic of the mask-assisted fabrication of all-solid-state planar EG-MSCs.

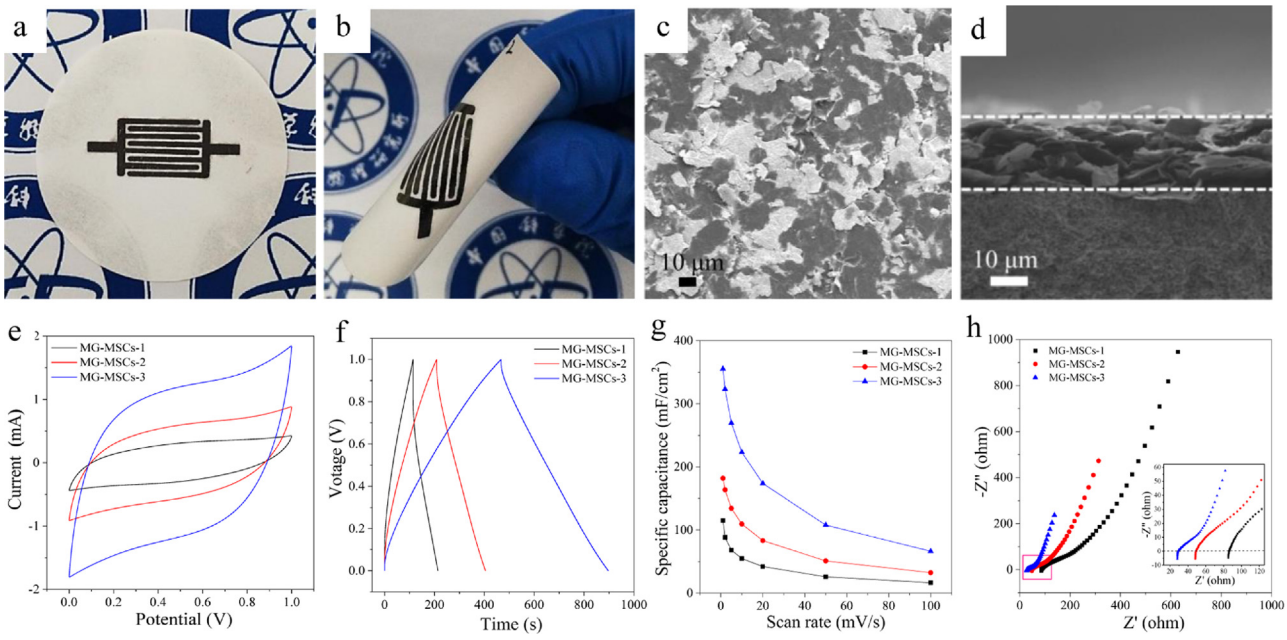

Fig. 3. Optical images of MG-MSCs taken at flat (a) and bending (b) states. Top-view SEM image of MG film. (d) Cross-section SEM images of MG film (2 mL dispersion of MnO_2 and EG). (e) CV curves tested at 20 mV/s. (f) GCD curves obtained at 0.2 mA/cm^2. (g) Areal capacitance as a function of scan rate. (h) EIS of MG-MSCs-1, MG-MSCs-2 and MG-MSCs-3.

nanosheets, with micrometer thickness of~19 μm, and a high electric conductivity of ~84 S/cm (Fig. 3d). This result indicated that the fabricated MG interdigital patterns could act as electrochemically active electrodes for MSCs.

The electrochemical behaviors of all-solid-state MG-MSCs-1, MG-MSCs-2 and MG-MSCs-3 based on MG films with varying mass loading were firstly evaluated by CV at different scan rate of 1–100 mV/s, GCD at a current density of 0.2 mA/cm, and EIS measurements. For comparison, we also fabricated EG-MSCs based on the pure EG films obtained by filtration of 2 mL EG dispersion while other steps were kept the same as MG-MSCs. Apparently, the CVs of MG-MSCs-1, MG-MSCs-2 and MG-MSCs-3 in comparison with EG-MSCs (Fig. S2 in Supporting information) showed the typical pseudocapacitive behavior originating from 2D MnO_2 nanosheets, and the increased current integration with increasing the volume of MnO_2 and EG dispersion from 1 mL to 2 mL and 4 mL (Fig. 3e). Similarly, this result was also confirmed by the GCD curves, which exhibited the stepwise discharge time, indicative of the increased areal capacitance (Fig. 3f). Further, GCD curves disclosed a small IR voltage drop and good reversibility of charge storage, indicative of high conductivity of MG films. The areal capacitance of MG-MSCs-1, MG-MSCs-2 and MG-MSCs-3 as a function of scan rate were shown in Fig. 3g. Remarkably, MG-MSCs-3 presented outstanding areal capacitance of 355 mF/cm^2 at a scan rate of 1 mV/s, which is much higher than those of MG-MSCs-1 (115 mF/cm^2), MG-MSCs-2 (182 mF/cm^2) and EG-MSCs (0.12 mF/cm^2), and is the highest value of the state-of-the-art MnO_2-based MSCs, such as Au/MnO_2/Au (11.9 mF/cm^2) [28], MnO_2 (225.2 mF/cm^2) [29], graphene fiber/MnO_2 (42.0 mF/cm^2) [30], carbon fiber/MnO_2//carbon fiber/MoO_3 (19.5 mF/cm^2) [31], graphene quantum dots//MnO_2 (4.4 mF/cm^2) [32] and superior to most reported graphene-based MSCs, *e.g.*, nanoporous activated graphene (89.5 mF/cm^2) [33] (Table S1 in Supporting information). Moreover, MG-MSCs-3 exhibited larger areal energy density (8.6 μWh/cm^2) and power density (575.7 μW/cm^2) than MG-MSCs-1 (2.8 μWh/cm^2 and 142.8 μW/cm^2), MG-MSCs-2 (4.4 μWh/cm^2 and 281.1 μW/cm^2) (Fig. S3 in Supporting information). Certainly, it should be mentioned that MG-MSCs-3 presented high areal capacitance of 66 mF/cm^2 at a high scan rate of 100 mV/s and kept 19% of initial capacitance at 1 mV/s, which demonstrated better rate capability than those of MG-MSCs-1 (16 mF/cm^2 at 100 mV/s, 14% of initial capacitance) and MG-MSCs-2 (32 mF/cm^2 at 100 mV/s, 18% of initial capacitance) (Fig. 3g). This enhanced rate capability can be well explained by the EIS spectroscopy (Fig. 3h). It was observed that the complex plane plots of MG-MSCs-3 displayed lower total resistance (including charge transport resistance) and larger slope than MG-MSCs-1 and MG-MSCs-2 at a low frequency (Fig. 3h). More importantly, MG-MSCs-3 showed a significantly decreased equivalent series resistance (ESR) of 28 Ω, which is much lower than those of MG-MSCs-1 (85 Ω) and MG-MSCs-2 (50 Ω), indicative of higher ion diffusion and electron transport in MG-MSCs-3.

To highlight the mechanical flexibility of MG-MSCs for microscale energy storage devices, we further evaluated the electrochemical performance of MG-MSCs under different bending angles and twisted state. It can be seen that the CV curves changed slightly at different bending degree (Fig. 4a) and severely twisted state (Fig. 4c), and 92% of initial capacitance for MG-MSCs-2 and 82% for MG-MSCs-3 at a flat stage was remained even at a highly bending angle of 180° (Fig. 4b and Fig. S4a in Supporting information), demonstrative of robust mechanical flexibility of MG-MSCs-2. Note that the better flexibility of MG-MSCs-2 over MG-MSCs-3 is mainly attributed to high mass loading of MG-MSCs-3. In addition, long-life cycling stability is an insistent requirement for supercapacitors. Fig. 4f showed the CV curves obtained at 200 mV/s as a function of the cycle number. Remarkably, the capacitance retention was maintained as high as ~95% after 3000 cycles for MG-MSCs-2 (Fig. 4g), which is better than MG-MSCs-3 (~80% after 3000 cycles, Fig. S4b in Supporting information). Overall, the superior electrochemical properties of MG-MSCs-2 was substantially attributed to the full optimization of

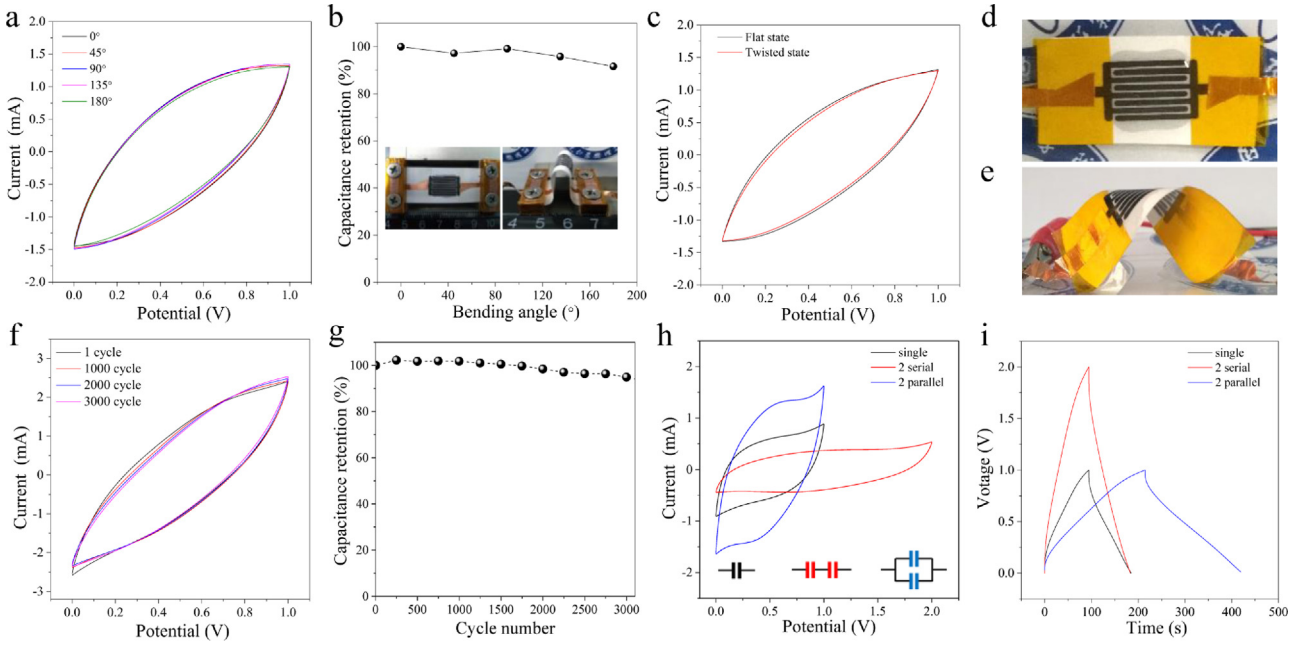

Fig. 4. (a) CV curves measured at 50 mV/s of MG-MSCs-2 under different bending angles. (b) Capacitance retention as a function of bending angle of MG-MSCs-2. Insets are optical images of MG-MSCs-2 taken at 0° and 180°. (c) CV curves measured at 50 mV/s of MG-MSCs-2 under flat and twisted state. (d, e) Optical images of MG-MSCs-2 taken under (d) flat and (e) twisted states. (f) The 1st, 1000th, 2000th and 3000th CV curves of MG-MSCs-2 obtained at 200 mV/s. (g) Cycling stability of MG-MSCs-2 for 3000 times obtained at 200 mV/s. (h) CV curves tested at 20 mV/s of single, 2 serial and 2 parallel interconnected MG-MSCs-2. (i) GCD curves obtained at 0.4 mA/cm^2 of single, 2 serial and 2 parallel interconnected MG-MSCs-2.

the suitable film thickness, coupling of 2D MnO_2 and EG nanosheets, and interfacial interaction of film electrode with elastic Nylon membrane substrate and aqueous gel electrolyte.

To meet the requirements for the integrated circuits, we further fabricated two MG-MSCs through serial or parallel connections to improve output voltage or capacitance. Fig. 4h showed two integrated MG-MSCs-2 in series or parallel, presenting increased output voltage from 1.0 V to 2.0 V or twofold capacitance. Similarly, the GCD curves obtained at a current density of 0.4 mA/cm^2 of two serial or parallel devices also validated sufficiently high applied voltage of 2.0 V or double current output (Fig. 4i). This result suggests that our MG-MSCs can be possibly coupled withthe desirable integrated circuit to satisfy variable voltage and current outputs.

Therefore, the outstanding performance of MG-MSCs can be attributed to rational design of MG film with an integrated synergetic effect of ultrathin pseudocapacitive MnO_2 nanosheets and high-conducting capacitive EG nanosheets: First, the layer-stacked film characterize high electronic conducting pathway of EG layer and 2D parallel ion channels between MnO_2 and EG layers, which can remarkably introduce additional pseudocapacitance and electrical double layer capacitance [34]. Second, the planar structures of MG film can offer more accessible electrochemically active surfaces and extra interface for fast ion absorption/desorption and rapid electron transport, leading to remarkable rate capability and cyclingstability [35]. Third, the densely packed film established by ultra-thinness and excellent mechanical flexibility of the 2D nanosheets is benefit for the significant improvement of the volumetric capacitance (97 F/cm^3) and the flexibility of planar MSCs [36].

In summary, we have demonstrated the fabrication of all-solid-state planar MG-MSCs based on interdigital patterned films of 2D pseudocapacitive MnO_2 nanosheets and capacitive EG using a universal simplified mask-assisted filtration technology. The as-produced MG-MSCs demonstrated impressive electrochemical performance, *e.g.*, high areal capacitance of 355 mF/cm^2, excellent mechanical flexibility as high as ~92% of initial capacitance even at a highly bending angle of 180°, outstanding cycling stability of 95% after 3000 cycles, and serial or parallelinterconnection for tailored voltage and capacitance. As a consequence, the rational fabrication of MSCs based on graphene and other 2D nanosheets with simplified electrode manufacturing technology will pave the ways for constructing next-generation high-performance, flexible, portable and wearable energy storage devices.

Acknowledgments

We gratefully acknowledge the financial support from the National Natural Science Foundation of China (No. 51572259), National Key R&D Program of China (Nos. 2016YBF0100100 and 2016YFA0200200), Thousand Youth Talents Plan of China, Natural Science Foundation of Liaoning Province (No. 201602737), and DICP (No. Y5610121T3), China Postdoctoral Science Foundation (Nos. 2016M601348 and 2016M601349) and dedicated funds for methanol conversion from DICP.

Appendix A. Supplementary data

Supplementary data associated with this article can be found, in the online version, at http://dx.doi.org/10.1016/j.cclet.2017.08.007.

References

[1] S. Zheng, Z.S. Wu, S. Wang, et al., Energy Storage Mater. 6 (2017) 70–97.
[2] Z.S. Wu, K. Parvez, X.L. Feng, K. Müllen, Nat. Commun. 4 (2013) 2487.
[3] Z.S. Wu, X. Feng, H.M. Cheng, Natl. Sci. Rev. 1 (2013) 277–292.
[4] Y. Gogotsi, P. Simon, Science 334 (2011) 917–918.
[5] I. Nam, G.P. Kim, S. Park, et al., Nanoscale 4 (2012) 7350–7353.
[6] X. Zhang, L. Hou, A. Ciesielski, P. Samori, Adv. Energy Mater. 6 (2016) 1600671.
[7] J.E. ten Elshof, H. Yuan, P. Gonzalez Rodriguez, Adv. Energy Mater. 6 (2016) 1600355.
[8] H. Zhang, ACS Nano 9 (2015) 9451–9469.
[9] B.S. Shen, H. Wang, L.J. Wu, et al., Chin. Chem. Lett. 27 (2016) 1586–1591.
[10] Y. Dong, Z.S. Wu, W. Ren, H.M. Cheng, X. Bao, Sci. Bull. 62 (2017) 724–740.
[11] X.F. Lin, Z.Y. Zhang, Z.K. Yuan, et al., Chin. Chem. Lett. 27 (2016) 1259–1270.

[12] L.Y. Liu, X. Zhang, H.X. Li, et al., Chin. Chem. Lett. 28 (2017) 206–212.
[13] Y. Dong, Z.S. Wu, S. Zheng, et al., ACS Nano 11 (2017) 4792–4800.
[14] M. Huang, F. Li, F. Dong, Y.X. Zhang, L.L. Zhang, J. Mater. Chem. A 3 (2015) 21380–21423.
[15] Z.P. Ma, G.J. Shao, Y.Q. Fan, et al., ACS Appl. Mater. Interfaces 8 (2016) 9050–9058.
[16] X. Huang, X. Qi, F. Boey, H. Zhang, Chem. Soc. Rev. 41 (2012) 666–686.
[17] L. Peng, X. Peng, B. Liu, et al., Nano Lett. 13 (2013) 2151–2157.
[18] S. Wang, Z.S. Wu, S. Zheng, et al., ACS Nano 11 (2017) 4283–4291.
[19] S. Zheng, Z. Li, Z.S. Wu, et al., ACS Nano 11 (2017) 4009–4016.
[20] Z.S. Wu, Y.Z. Tan, S. Zheng, et al., J. Am. Chem. Soc. 139 (2017) 4506–4512.
[21] R. Li, Y. Wang, C. Zhou, et al., Adv. Funct. Mater. 25 (2015) 5384–5394.
[22] R. Li, Y. Wang, C. Zhou, et al., Adv. Sci. 4 (2017) 1600539.
[23] D.P. Dubal, J.G. Kim, Y. Kim, et al., Energy Technol. 2 (2014) 325–341.
[24] Y. Liu, X. Miao, J. Fang, et al., ACS Appl. Mater. Interfaces 8 (2016) 5251–5260.
[25] K. Kai, Y. Yoshida, H. Kageyama, et al., J. Am. Chem. Soc. 130 (2008) 15938–15943.
[26] J. Zhang, J. Jiang, X.S. Zhao, J. Phys. Chem. C 115 (2011) 6448–6454.
[27] S. Rong, P. Zhang, Y. Yang, et al., ACS Catal. 7 (2017) 1057–1067.
[28] H. Hu, Z. Pei, H. Fan, C. Ye, Small 12 (2016) 3059–3069.
[29] X. Wang, B.D. Myers, J. Yan, et al., Nanoscale 5 (2013) 4119–4122.
[30] X. Li, T. Zhao, Q. Chen, et al., Phys. Chem. Chem. Phys. 15 (2013) 17752–17757.
[31] J. Noh, C.M. Yoon, Y.K. Kim, J. Jang, Carbon 116 (2017) 470–478.
[32] W.W. Liu, Y.Q. Feng, X.B. Yan, J.T. Chen, Q.J. Xue, Adv. Funct. Mater. 23 (2013) 4111–4122.
[33] Z.S. Wu, S. Yang, L. Zhang, et al., Energy Storage Mater. 1 (2015) 119–126.
[34] Z.S. Wu, W.C. Ren, D.W. Wang, et al., ACS Nano 4 (2010) 5835–5842.
[35] Z.S. Wu, K. Parvez, A. Winter, et al., Adv. Mater. 26 (2014) 4552–4558.
[36] M.J. Shi, S.Z. Kou, B.S. Shen, et al., Chin. Chem. Lett. 25 (2014) 859–864.